Remote Sensing of Soil Moisture and Vegetation Status Using Space-Borne GNSS-R Observations

Mina Rahmani *, Jamal Asgari

Dept. of Geomatics Engineering, Faculty of Civil Engineering and Transportation, University of Isfahan, Isfahan, Iran - (mi.rahmani, asgari) @eng.ui.ac.ir

KEY WORDS: GNSS Reflectometry (GNSS-R), Bi-static radar, CYGNSS, Soil moisture, Vegetation status, Soil surface roughness.

ABSTRACT:

Recently, GNSS Reflectometry (GNSS-R) has gained increasing attention for remote sensing and hydrological applications, particularly in monitoring soil moisture and vegetation status. As a novel bi-static radar technique, GNSS-R utilizes GNSS signals (e.g., GPS) reflected off the Earth's surface, which carry valuable information about surface conditions. However, applying this technique to remote sensing is not straightforward, as GNSS-R observations are influenced by several factors, including instrumental and geometrical parameters. This paper aims to demonstrate the sensitivity of NASA's GNSS-R mission, Cyclone GNSS (CYGNSS), to soil moisture variations and to investigate the influence of vegetation status—using vegetation water content (VWC), Leaf Area Index (LAI) and canopy height as indicators—soil surface roughness, and incidence angle on these observations. Our results show good agreement between CYGNSS observations and SMAP soil moisture, with sensitivity decreasing at larger incidence angles (60–70°) and higher VWC (dense vegetation). Additionally, CYGNSS reflectivity exhibits a strong negative correlation with vegetation indicators, including VWC ($R \approx -0.8$), LAI ($R = -0.9346$), and canopy height ($R = -0.9795$), highlighting its effectiveness in monitoring vegetation status. This negative correlation, along with the observed strong negative correlation coefficients (≤ -0.8) between CYGNSS reflectivity and the SMAP-provided surface roughness parameter (Hr), confirms the attenuation of microwave signals caused by dense vegetation and soil surface roughness.

1. INTRODUCTION

According to the Global Climate Observing System (GCOS), soil moisture is one of the Essential Climate Variables (ECVs). This variable plays a key role in hydrological processes, agriculture, and the prediction of floods, droughts, and vegetation status (Duan et al., 2024; Akash et al., 2024).

Microwave remote sensing missions, which operate based on the measurement of natural radiation from the Earth's surface—such as the Soil Moisture Active and Passive (SMAP) mission (Entekhabi et al., 2014) and the Soil Moisture Ocean Salinity (SMOS) mission (Kerr et al., 2012)—have been widely used for global soil moisture monitoring. However, these missions face limitations in spatial resolution, with a coarse sampling rate of approximately 40 km, and provide observations only every 2–3 days.

Recently, the GNSS Reflectometry (GNSS-R) technique has gained increasing attention for remote sensing and hydrological applications, including soil moisture and vegetation status monitoring. As a novel and innovative bi-static radar method, GNSS-R utilizes GNSS signals (e.g., GPS) reflected off the Earth's surface, which carry valuable information about surface conditions (Rahmani et al., 2022). Figure 1 illustrates the fundamental differences between microwave remote sensing and the GNSS-R technique.

GNSS-R has seen increasing adoption for soil moisture retrieval, driven by its many advantages (Rahmani et al., 2022). Notably, the growing availability of GNSS systems and signals, combined with the capability of affordable GNSS-R receivers to simultaneously monitor multiple reflected signals, enables GNSS-R to achieve superior spatio-temporal resolution —providing hourly and daily observations with spatial resolutions ranging from 1 to 25 km—compared to traditional soil moisture remote sensing satellites (Rahmani et al., 2025). The sensitivity of L-band GNSS signals to soil moisture variations offers an additional advantage.

The primary observation of the GNSS-R technique are two-dimensional maps called Delay Doppler Maps (DDMs). These maps represent reflected power over the areas surrounding the GNSS signal's point of incidence on the Earth's surface, as a function of delay and Doppler shift. The shape of these maps and the power values depend on several factors, including soil moisture and soil surface roughness.

* Corresponding author

Figure 2 shows two samples of DDMs from two distinct case studies.

To date, the effectiveness of GNSS-R observations in soil moisture monitoring has been demonstrated in several studies (e.g., Al-Khaldi et al., 2019). For instance, Chew et al. (2016) reported a strong agreement between GNSS-R Signal-to-Noise Ratio (SNR) and SMOS-derived soil moisture. Additionally, research by Chew and Small (2018) found correlation coefficients exceeding 0.7 across most regions globally.

However, applying this technique to remote sensing and hydrological studies is not straightforward, as its observations depend on several factors, including instrumental and geometrical parameters as well as the Earth condition. This paper, aim to demonstrate the sensitivity of NASA's GNSS-R mission, Cyclone GNSS (CYGNSS), to soil moisture variations and investigate the influence of vegetation status, incidence angle (as one of the key geometrical factors) and soil surface roughness on these observations.

The paper is organized in the following way: Section 2 is devoted to the datasets employed in this study. Section 3 outlines the methodology used; Section 4 presents the results; and finally, Section 5 provides the conclusions.

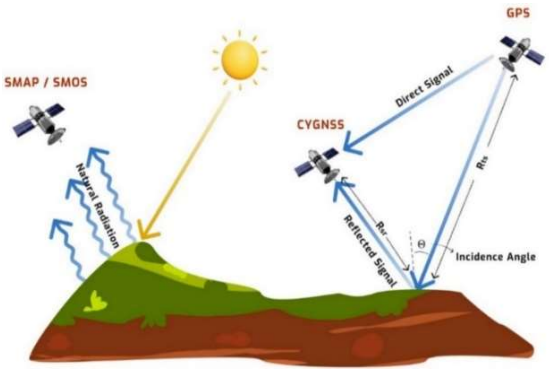

Figure 1. The basic principles of microwave remote sensing (SMAP and SMOS) and the GNSS-R technique.

2. METHODOLOGY

CYGNSS reflectivity (Γ_{eff}) is calculated from CYGNSS Level 1 observations, following the methodology outlined by Rahmani et al. (2025):

$$\Gamma_{eff}(\theta) = \frac{\tilde{P}_r^S (4\pi)^2 (R_{ts}+R_{sr})^2}{\lambda^2 \, P_t \; G_t \, G_r} \quad (1)$$

The description of the variables in Equation 1 is provided in Table 1.

$\tilde{P}_r^S = P_r - P_N$, where P_r represents the strength of the central signal in the CYGNSS Delay-Doppler Map, while P_N denotes the noise power estimated from the first two Doppler bins within the DDM.

The following equation models the influence of vegetation (via vegetation optical depth (τ_{NAD}), which is assumed to be linearly correlated with VWC) and soil surface roughness (via H_{RP}) on CYGNSS reflectivity values, as discussed by Yueh et al. (2020):

$$\Gamma_{eff} = \left(\exp\left(-\frac{2\tau_{NAD}}{cos\theta}\right)\exp\left(\frac{-H_{RP}(\theta)}{\cos\theta}\right)\right)|R|^2 \quad (2)$$

Where reflection from a smooth surface, Fresnel reflectivity ($|R|^2$), can be obtain using the Fresnel equations, which requires soil permittivity (ε_{r}) and incidence angle) and θ (as inputs:

$$R_{\text{lr}} = R_{\text{rl}} = \frac{1}{2}(R_{\text{vv}} - R_{\text{hh}}) \quad (3)$$

$$R_{\text{hh}}(\theta) = \frac{\cos\theta - \sqrt{\varepsilon_{\text{r}} - \sin^2\theta}}{\cos\theta + \sqrt{\varepsilon_{\text{r}} - \sin^2\theta}} \quad (4)$$

$$R_{\text{vv}}(\theta) = \frac{\varepsilon_{\text{r}}\cos\theta - \sqrt{\varepsilon_{\text{r}} - \sin^2\theta}}{\varepsilon_{\text{r}}\cos\theta + \sqrt{\varepsilon_{\text{r}} - \sin^2\theta}} \quad (5)$$

Variable	Definition
P_{r}^{t}	Transmitted power
G^{t}	Transmitter antenna gain
G^{r}	Receiver antenna gain
R_{ts}	Distance between transmitter and specular point (incidence point of GPS signals on the Earth)
R_{sr}	Distance between specular point and receiver
λ	L-band wavelength (19.6 cm)

Table 1. Definition of the variables in Equation 1.

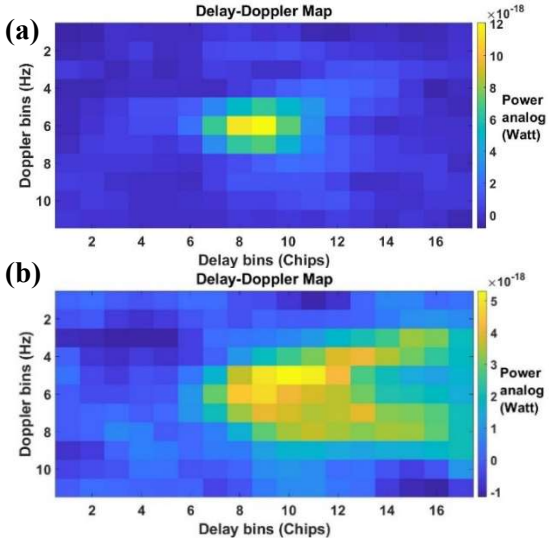

Figure 2. Sample of DDM over (a) the Indian Ocean and (b) an agricultural region in China.

Soil permittivity is linked to the value of soil moisture (m_v) through the equations described by (Tabbagh et al., 2000; Topp et al., 1980):

$$m_v = -5.3 \times 10^{-2} + 2.92 \times 10^{-2}\varepsilon_r - 5.5 \times 10^{-4}{\varepsilon_r}^2 + 4.3 \times 10^{-6}{\varepsilon_r}^3 \quad (6)$$

$$\varepsilon_r = 3.1 + 17.36m_v + 63.12\, m_v^2 + j(0.031 + 4.65m_v + 20.42m_v^2) \quad (7)$$

3. DATASETS

3.1 CYGNSS

The Cyclone Global Navigation Satellite System (CYGNSS) is a constellation of small CubeSat satellites launched into orbits with a 580 km altitude and a 35-degree inclination by NASA in late 2016. Initially, the mission was designed for cyclone monitoring over tropical regions; therefore, it covers latitudes ranging from 37°N to 37°S, which experience most cyclones. Each satellite carries two L-band antennas pointing toward the nadir to receive GPS signal reflections and one zenith-facing antenna to detect direct GPS signals. Each satellite can measure up to four reflections at once. With eight observatories in operation, 32 DDMs are generated every second. As a result, CYGNSS achieves remarkably high temporal sampling rates, averaging 7.2 hours over oceanic regions and approximately 1 to 2 days over land surfaces (Ruf et al., 2016; Rahmani et al., 2022).

However, CYGNSS, like any other mission, has its drawbacks. Among all GNSS constellations (e.g., GPS, Galileo, GLONASS), CYGNSS measurements are restricted to GPS observations. The mission only covers regions between 37° north and 37° south latitude and cannot provide observations for areas such as Europe. To mitigate these limitations, the European Space Agency (ESA) plans to launch the HydroGNSS mission in October 2025, which will offer global coverage and measure reflections from both GPS and Galileo satellites (Unwin et al., 2021). Additionally, due to the motion of both the transmitters (GPS satellites) and the receivers (CYGNSS satellites), the distribution of specular points—the locations on Earth's surface where GNSS signals reflect toward the receiver—is inherently random. Figure 3 illustrates an example of the specular point distribution measured by one of the eight CYGNSS satellites.

For this study, we collected the CYGNSS Level 1 dataset from the Physical Oceanography Distributed Active Archive Center (PO.DAAC)[2].

3.2 SMAP SM and VWC

Launched by NASA in January 2015, SMAP is an L-band microwave remote sensing mission designed to monitor Earth's surface characteristics (Wigneron et al., 2017). The mission was originally intended to deploy a passive radiometer and an active synthetic radar antenna to take advantage of both active and passive microwave systems for soil moisture monitoring. However, the active system stopped functioning on July 7, 2015, leaving only the passive instrument to continue collecting data (Entekhabi et al., 2014).

This study utilized the SMAP Level 3 dataset (SPL3SMPE) (O'Neill et al., 2018), accessible via https://nsidc.org/data/spl3smp_e/versions/6, to retrieve soil moisture information. The dataset delivers global estimates of soil moisture with a precision of 0.04 m^3/m^3, is spatially interpolated to a 9 km grid, and supports daily monitoring of surface soil moisture in the top 0–5 cm layer (Chan and Dunbar, 2019). Furthermore, VWC data provided in the SMAP observation files were utilized. VWC represents the quantity of water retained within vegetation and plays a vital role in assessing plant water stress (Asgarimehr et al., 2024).

3.3. Other Datasets

To investigate the sensitivity of CYGNSS observations to vegetation conditions, two additional datasets were employed in this study: the ERA5-Land Leaf Area Index (LAI), provided by the European Centre for Medium-Range Weather Forecasts (ECMWF) (Muñoz Sabater, 2019), and the Global Forest Canopy Height (CH) dataset, derived from ICESat/GLAS lidar observations, which provides global estimates of canopy height at a 1 km resolution (Simard et al., 2011).

4. RESULTS

In this section, we first examine the influence of incidence angle on simulated reflectivity values. Subsequently, we analyze the sensitivity of CYGNSS observations to variations in soil moisture. The last two subsections are devoted to the influence of vegetation status and soil surface roughness on CYGNSS observations.

4.1 The Impact of Incidence Angle on Fresnel Reflectivity

We investigate the impact of incidence angle on Fresnel reflectivity, simulated using the Fresnel equations (Equations 3–5), across four distinct ranges of soil moisture. As illustrated in Figure 4, Fresnel reflectivity exhibits minimal variation within each soil moisture range for incidence angles below 60 degrees. However, for angles exceeding 60 degrees, reflectivity decreases progressively with increasing incidence angle.

4.2 Sensitivity of CYGNSS Observation to Soil Moisture

Figure 5(a) illustrates the sensitivity of CYGNSS reflectivity on the 5th day of 2020, at a global scale, to SMAP soil moisture values across three ranges of incidence angles (20–30°, 40–50°, and 60–70°). Statistical analysis of the data illustrated in Figure 5, as summarized in Table 2, reveals that

[2] https://podaac.jpl.nasa.gov/CYGNSS?tab=mission

for incidence angles between 20° and 30°, the correlation exceeds 0.8 across all VWC intervals..

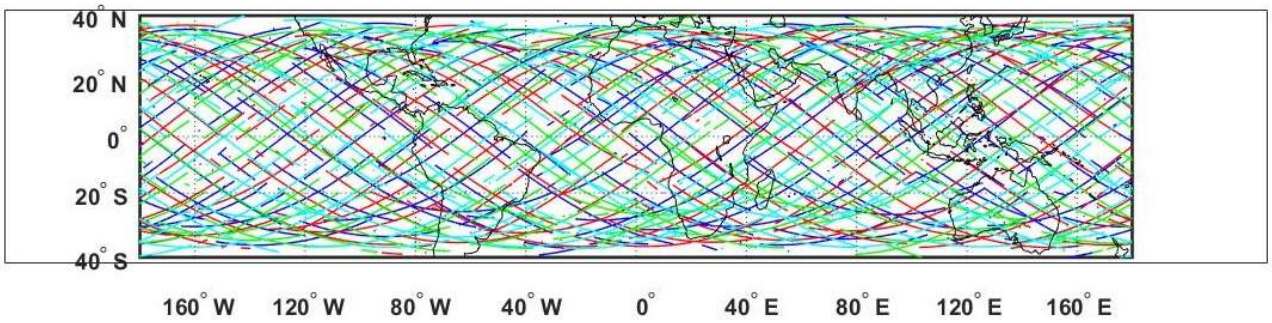

Figure 3. Distribution of specular points measured by one of the eight satellites of the CYGNSS mission. Each color represents one of the four groups of reflections measured by this satellite.

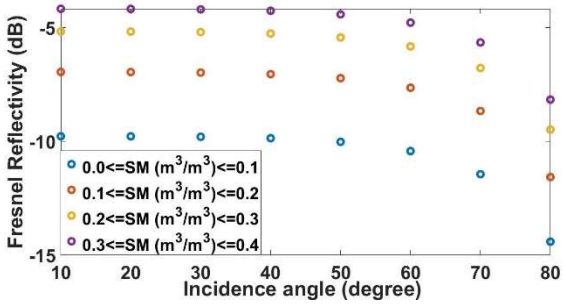

Figure 4. Fresnel reflectivity versus incidence angle for different range of soil moisture.

Also for the 40–50° group, CYGNSS observations show strong and statistically significant correlations with soil moisture across most intervals (e.g., R > 0.9 and p-values near zero), indicating high sensitivity to soil moisture. However, in the highest VWC range (15–18 kg/m²), the correlation becomes negative (R = –0.4274), suggesting signal attenuation caused by dense vegetation structure. In contrast, the 60–70° group demonstrates less consistent behavior. While the lowest VWC range (0–3 kg/m²) still shows a strong correlation (R = 0.9234), the remaining intervals yield weak or even negative correlations, with some p-values indicating statistical insignificance. This suggests that at higher incidence angles, CYGNSS sensitivity to soil moisture diminishes, likely due to increased signal scattering and geometric effects.

In addition to correlation coefficients, the slope values in Table 2 highlight how CYGNSS reflectivity responds to changes in soil moisture under varying observation geometries and vegetation conditions. At low incidence angles (20–30°), the slope reaches its peak (22.18 dB·m³/m³) in the 3–6 kg/m² VWC range, indicating strong sensitivity. In comparison, the 40–50° group shows slightly reduced slopes overall, particularly at higher VWC levels, suggesting a moderate decline in sensitivity. At high incidence angles (60–70°), slope values become inconsistent and negative, especially under dense vegetation, reflecting diminished signal reliability likely due to increased scattering and attenuation effects.

The sensitivity of CYGNSS reflectivity to temporal soil moisture changes has been investigated over the contiguous United States (CONUS), as shown in Figure 6(a). Figure 6(b) presents a time series comparison between CYGNSS reflectivity (in dB, blue line) and SMAP soil moisture (in m³/m³, red dashed line) from March 2020 to June 2021, indicating a positive correlation (R = 0.65), where higher reflectivity values generally correspond to higher soil moisture levels. This demonstrates the effectiveness of CYGNSS observations in capturing temporal variations in soil moisture provided by SMAP.

4.3 Sensitivity of CYGNSS Reflectivity to Vegetation Status

Figure 7 illustrates the high sensitivity of CYGNSS reflectivity, on the 5th day of 2020 at a global scale, to vegetation status—using SMAP VWC as an indicator—for incidence angles between 20° and 30°. The figure shows that CYGNSS reflectivity values decrease as VWC increases. Figure 8(a) presents the correlation coefficient between CYGNSS reflectivity and SMAP VWC for three incidence angle ranges—20–30°, 40–50°, and 60–70°—on a global scale for the 5th day of 2020. The results show correlation coefficients exceeding –0.7 in magnitude across all soil moisture and incidence angle ranges, indicating a strong sensitivity of CYGNSS reflectivity to spatial variations in VWC. These correlation coefficients slightly decrease as the incidence angle increases.

Figure 8(b) shows the correlation coefficients between CYGNSS reflectivity and SMAP VWC for the year 2020 over the CONUS, evaluated across three ranges of incidence angle and soil moisture. All coefficients exceed -0.9,

confirming the strong sensitivity of CYGNSS reflectivity to variations in SMAP VWC.

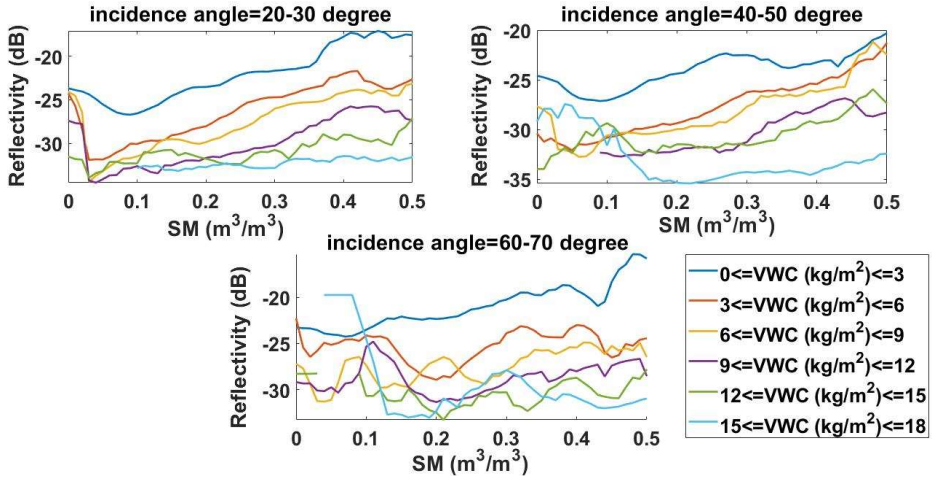

Figure 5. (a) Sensitivity of CYGNSS reflectivity to SMAP soil moisture values, and (b) polar plot of the corresponding correlation coefficients across different ranges of VWC and three incidence angle groups.

Incidence angle (degree)	VWC (kg/m²)	R	p-value	Slope (dB m3/ m3)
20-30	0-3	0.9350	0.0001	18.95
	3-6	0.9663	0.0000	22.18
	6-9	0.8318	3.986e-14	17.51
	9-12	0.8303	4.879e-14	15.21
	12-15	0.8187	2.157e-13	7.69
	15-18	0.8353	1.108e-11	3.60
40-50	0-3	0.8385	1.606e-14	10.01
	3-6	0.9782	0.0000	19.21
	6-9	0.8703	1.093e-16	17.34
	9-12	0.9145	1.033e-17	14.93
	12-15	0.7615	8.682e-11	9.41
	15-18	-0.4274	0.0017	-
60-70	0-3	0.9234	0.0000	14.63
	3-6	0.1973	0.1651	-
	6-9	0.7219	2.251e-09	8.59
	9-12	0.2854	0.0422	-
	12-15	0.0289	0.8486	-
	15-18	-0.5260	0.0002	-14.86

Table 2. Correlation coefficient (R), p-value, and regression slope between CYGNSS reflectivity and SMAP soil moisture across three incidence angle groups and six VWC intervals.

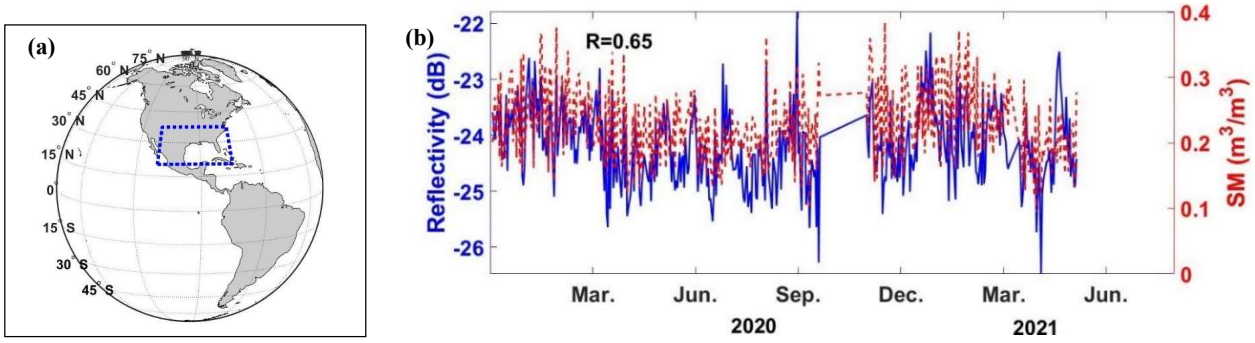

Figure 6. (a) Case study area indicated by blue dashed lines over CONUS. (b) Time series of CYGNSS reflectivity versus SMAP soil moisture.

This contribution has been peer-reviewed. The double-blind peer-review was conducted on the basis of the full paper.
https://doi.org/10.5194/isprs-annals-X-4-W8-2025-601-2026 | © Author(s) 2026. CC BY 4.0 License.

Additionally, the observed strong correlation coefficients between CYGNSS reflectivity and LAI (R =–0.9346), and canopy height (R =–0.9795) on a global scale, Figure 9, confirm the effectiveness of CYGNSS reflectivity in monitoring vegetation status.

4.4 The Influence of Soil Surface Roughness on CYGNSS Reflectivity

Figure 10 investigates the sensitivity of CYGNSS reflectivity to spatial variations in the SMAP-provided surface roughness parameter (Hr) across different ranges of VWC on four distinct days in 2020.

Across all VWC ranges, reflectivity decreases as SMAP Hr increases, indicating a negative correlation between surface roughness and observed reflectivity. This behavior is consistent with expectations, as smoother surfaces (lower Hr) lead to higher specular reflection, while rougher surfaces (higher Hr) scatter the signal more, reducing the observed reflectivity. According to Figure 11, which presents the correlation coefficients between CYGNSS reflectivity and SMAP Hr values corresponding to the regression shown in Figure 10, we observed that the correlation coefficients are generally stronger than –0.8.

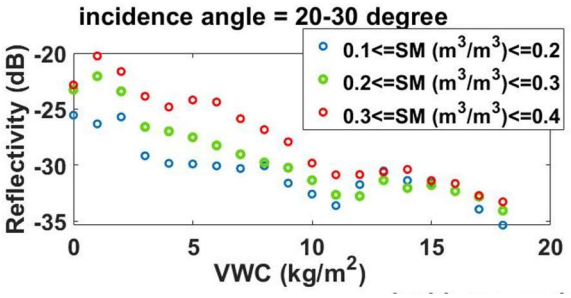

Figure 7. CYGNSS reflectivity versus SMAP VWC for an incidence angle of 20–30 degrees and three ranges of soil moisture on the 5th day of 2020, at a global scale.

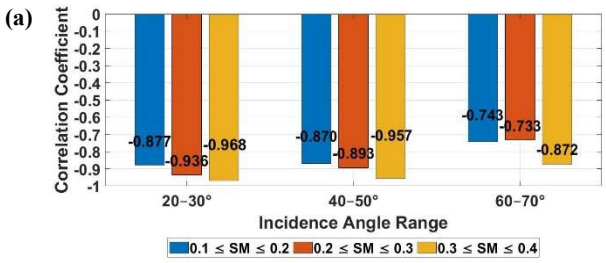

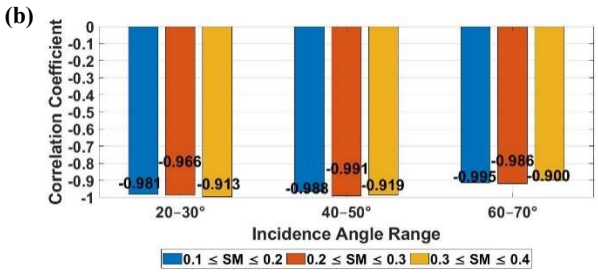

Figure 8. Correlation coefficient between CYGNSS reflectivity and SMAP VWC for three incidence angle ranges—20–30°, 40–50°, and 60–70°—(a) on a global scale for the 5th day of 2020, (b) over the conus for the whole year 2020.

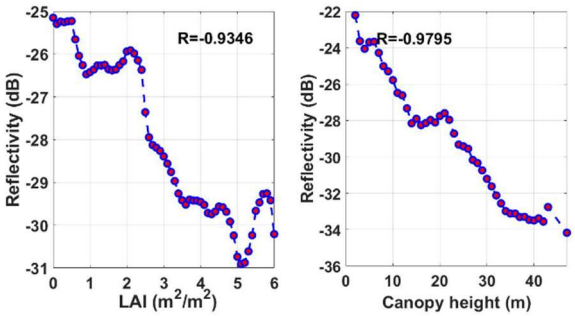

Figure 9. CYGNSS reflectivity versus LAI and canopy height.

5. CONCLUSIONS

This study demonstrated the potential of NASA's CYGNSS mission for monitoring soil moisture and vegetation status using spaceborne GNSS-R observations. The results revealed good agreement between CYGNSS reflectivity and SMAP-derived soil moisture, particularly at lower incidence angles (< 60°), confirming the high sensitivity of GNSS-R signals to near-surface soil moisture variations. However, this sensitivity diminishes under dense vegetation canopies and at larger incidence angles due to increased scattering and attenuation effects.

The analysis also highlighted a strong negative correlation between CYGNSS reflectivity and vegetation indicators, including vegetation water content (VWC), leaf area index (LAI), and canopy height. These results indicate that CYGNSS observations effectively capture vegetation dynamics and canopy structure. Moreover, the study confirmed that both vegetation attenuation and soil surface roughness significantly reduce reflectivity, emphasizing the necessity of accounting for these biophysical and surface parameters in GNSS-R retrieval models.

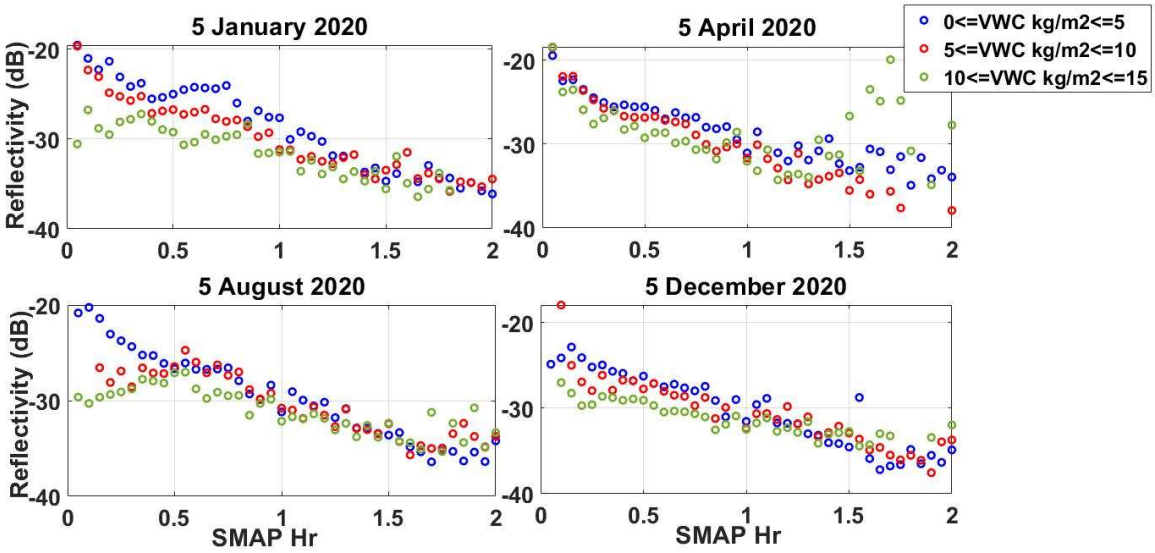

Figure 10. CYGNSS reflectivity versus SMAP Hr for three VWC ranges—0–5, 5–10, and 10–15 kg/m²—on a global scale for (a) 5 January 2020, (b) 5 April 2020, (c) 5 August of 2020 and (d) 5 December of 2020.

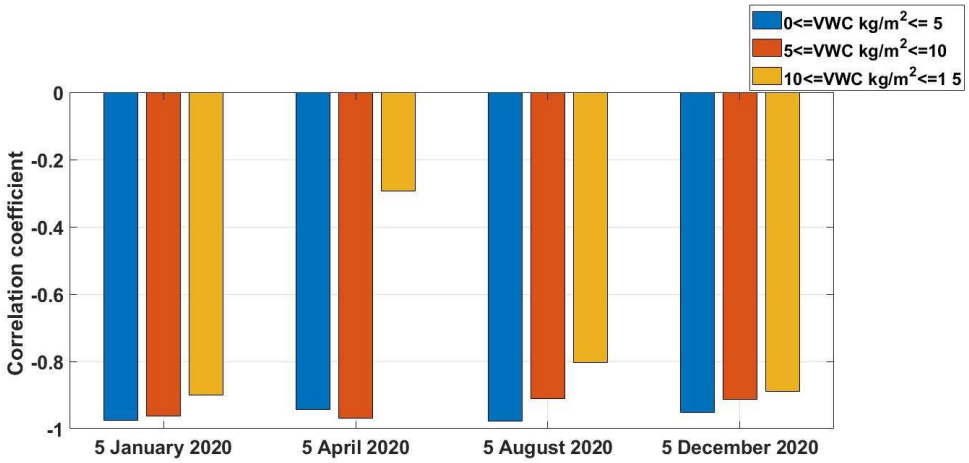

Figure 11. Correlation coefficients between CYGNSS reflectivity and SMAP-provided Hr values, based on the regressions shown in Figure 10.

Overall, the analysis underscores the promise of CYGNSS and GNSS-R techniques as complementary tools to traditional microwave missions such as SMAP, offering finer spatio-temporal resolution for hydrological and agricultural applications.

ACKNOWLEDGEMENTS

The authors are thankful to NASA's CYGNSS and SMAP teams for providing the public datasets.

REFERENCES

Akash, M., Kumar, P.M., Bhaskar, P., Deepthi, P., Sukhdev, A., 2024. Review of estimation of soil moisture using active microwave remote sensing technique. *Remote Sens. Appl.: Soc. Environ*., 33, 101118.

Al-Khaldi, M.M., Johnson, J.T., O'Brien, A.J., Balenzano, A., Mattia, F., 2019. Time-series retrieval of soil moisture using CYGNSS. *IEEE Trans. Geosci. Remote Sens*., 57(7), 4322–4331.

Asgarimehr, M., Entekhabi, D., Camps, A., 2024. Diurnal vegetation moisture cycle in the Amazon and response to water stress. *Geophys. Res. Lett*., 51(19), e2024GL111462.

Chan, S., Dunbar, S., 2019. Level 3 passive soil moisture product specification document. Tech. Rep. JPL.

Chew, C., Shah, R., Zuffada, C., Hajj, G., Masters, D., Mannucci, A.J., 2016. Demonstrating soil moisture remote sensing with observations from the UK TechDemoSat-1 satellite mission. *Geophys. Res. Lett*., 43(7), 3317–3324.

Chew, C., Small, E., 2018. Soil moisture sensing using spaceborne GNSS reflections: Comparison of CYGNSS reflectivity to SMAP soil moisture. *Geophys. Res. Lett*., 45(9), 4049–4057.

Duan, X., Maqsoom, A., Khalil, U., Aslam, B., Amjad, T., Tufail, R.F., Tariq, A., 2024. Enhancing soil moisture retrieval in semi-arid regions using machine learning algorithms and remote sensing data. *Appl. Soil Ecol*., 204, 105687.

Entekhabi, D., Yueh, S., O'Neill, P.E., Kellogg, K.H., Allen, A., Bindlish, R., et al., 2014. SMAP handbook–soil moisture active passive: Mapping soil moisture and freeze/thaw from space.

Kerr, Y.H., Waldteufel, P., Richaume, P., Wigneron, J.P., Ferrazzoli, P., Mahmoodi, A., et al., 2012. The SMOS soil moisture retrieval algorithm. *IEEE Trans. Geosci. Remote Sens*., 50(5), 1384–1403.

Muñoz Sabater, J., 2019. ERA5-Land hourly data from 1950 to present. Copernicus Climate Change Service (C3S) Climate Data Store (CDS).

Rahmani, M., Asgari, J., Asgarimehr, M., 2022. Soil moisture retrieval using space-borne GNSS reflectometry: a comprehensive review. *Int. J. Remote Sens*., 43(14), 5173–5203.

Rahmani, M., Asgari, J., Asgarimehr, M., Wickert, J., 2025. Investigation of the global influence of surface roughness on space-borne GNSS-R observations. *J. Geophys. Res. Biogeosci*., 130(3), e2024JG008243.

Ruf, C. S., Atlas, R., Chang, P. S., Clarizia, M. P., Garrison, J. L., Gleason, S., et al., 2016. New ocean winds satellite mission to probe hurricanes and tropical convection. Bulletin of the American Meteorological Society, 97(3), 385-395.

Tabbagh, A., Camerlynck, C., Cosenza, P., 2000. Numerical modeling for investigating the physical meaning of the relationship between relative dielectric permittivity and water content of soils. *Water Resour. Res*., 36(9), 2771–2776.

Simard, M., Pinto, N., Fisher, J. B., Baccini, A., 2011. Mapping forest canopy height globally with spaceborne lidar. *J. Geophys. Res. Biogeosci.* 116(G4).

Topp, G.C., Davis, J.L., Annan, A.P., 1980. Electromagnetic determination of soil water content: Measurements in coaxial transmission lines. *Water Resour. Res*., 16(3), 574–582.

Unwin, M.J., Pierdicca, N., Cardellach, E., Rautiainen, K., Foti, G., Blunt, P., Tossaint, M., 2021. An introduction to the HydroGNSS GNSS reflectometry remote sensing mission. *IEEE J. Sel. Top. Appl. Earth Obs. Remote Sens.*, 14, 6987–6999.

Wigneron, J.-P., Jackson, T., O'Neill, P., De Lannoy, G., de Rosnay, P., Walker, J., Grant, J., 2017. Modelling the passive microwave signature from land surfaces: A review of recent results and application to the L-band SMOS & SMAP soil moisture retrieval algorithms. *Remote Sens. Environ*., 192, 238–262.

Yueh, S.H., Shah, R., Chaubell, M.J., Hayashi, A., Xu, X., Colliander, A., 2020. A semiempirical modeling of soil moisture, vegetation, and surface roughness impact on CYGNSS reflectometry data. *IEEE Trans. Geosci. Remote Sens*., 60, 1–17.